Obrabotka metallov (tekhnologiya, oborudovanie, instrumenty) = Metal Working and Material Science. 2026 vol. 28 no. 2 pp. 280–297
ISSN: 1994-6309 (print) / 2541-819X (online)
DOI: 10.17212/1994-6309-2026-28.2-280-297

NSTU NETI

Obrabotka metallov - Metal Working and Material Science

Journal homepage: http://journals.nstu.ru/obrabotka_metallov

Manufacturing of die components from WC–15Co and WC–5Fe–5Ni–5Co alloys using dies obtained by photopolymer 3D printing

Maksim Dvornik [a], ***Elena Mikhailenko*** [b], ***Nuriya Vlasova*** [c]

Khabarovsk Federal Research Center of the Far Eastern Branch of the Russian Academy of Sciences, 153 Tikhookeanskaya Str., Khabarovsk, 680042, Russian Federation

[a] https://orcid.org/0000-0002-1216-4438, maxxxx80@mail.ru; [b] https://orcid.org/0000-0002-4515-9109, mea80@list.ru;
[c] https://orcid.org/0000-0003-0198-0912, Vlasova64@yandex.ru

ARTICLE INFO

Article history:
Received: 18 February 2026
Revised: 26 February 2026
Accepted: 23 March 2026
Available online: 15 June 2026

Keywords:
Cemented carbide
Die
Cutting insert
Medium-entropy binder phase
Wear resistance

Funding
The study was carried out under the state assignment of the Ministry of Science and Higher Education of the Russian Federation No. 075-00399-26-00.

ABSTRACT

Introduction. Manufacturing steel or carbide dies is an expensive process, significantly impacting the cost of powder metallurgy products, especially in pilot and small-scale production. A promising direction is the use of additive manufacturing for tooling fabrication and the application of alternative, less expensive binders for cemented carbides. ***The purpose of this work*** is to investigate the feasibility of using additive manufacturing for forming die blanks from *WC–15 Co* and *WC–5 Fe–5 Ni–5 Co* cemented carbides and to conduct a comparative analysis of their phase composition, microstructure, density, hardness, fracture toughness, strength, and wear resistance. **Methods.** Die components (dies and punches) made of *WC–15 Co* and *WC–5 Fe–5 Ni–5 Co* alloys were fabricated by cold pressing of granulated powders in dies obtained by photopolymer 3D printing (*Water-Wash Resin 2.0*, layer height 20 μm), followed by vacuum sintering at 1,400 °C. A comparative analysis was performed to evaluate the density, phase composition, microstructure, hardness, strength, fracture toughness, and microabrasive wear resistance of the obtained materials. Using the experimental cemented carbide dies, *SNUM-120408* cutting inserts made of *WC–6 Co* cemented carbide were produced by cold pressing and sintering at 1,450 °C. The insert dimensions were compared with the requirements of *GOST 19052-80*, *GOST 19042-80* and a commercial counterpart. **Results and Discussion.** The fundamental feasibility of manufacturing large-sized cemented carbide die components (weighing up to 210 g) using photopolymer tooling has been experimentally confirmed. The relative density of the components was 99.1% for *WC–15 Co* and 98.3% for *WC–5 Fe–5 Ni–5 Co*, which is slightly lower than that of reference samples pressed at higher pressure in a steel die. It is shown that replacing the cobalt binder with a medium-entropy *Fe–Ni–Co* binder suppresses *WC* grain growth (average grain size: 1.18 μm vs. 1.40 μm). This, together with the higher hardness of the binder, results in increased alloy hardness (1,070 HV vs. 1,010 HV) and a 10% reduction in the microabrasive wear rate. The manufactured dies produced cutting inserts whose geometric parameters (cutting edge length, thickness, corner radius) and physical and mechanical properties comply with the requirements of *GOST 19052-80* and *GOST 3882-74* and are comparable to commercial counterparts. **Conclusion.** The proposed approach, combining low-cost photopolymer 3D printing for tooling fabrication with the use of a medium-entropy *Fe–Ni–Co*-bonded cemented carbide, enables the efficient production of functional cemented carbide dies for small-scale production. The *WC–5 Fe–5 Ni–5 Co* cemented carbide, exhibiting higher hardness and wear resistance, is a promising alternative to the standard *WC–15 Co* cemented carbide for these operating conditions.

For citation: Dvornik M.I., Mikhailenko E.A., Vlasova N.M. Manufacturing of die components from WC-15Co and WC-5Fe-5Ni-5Co alloys using dies obtained by photopolymer 3D printing. *Obrabotka metallov (tekhnologiya, oborudovanie, instrumenty) = Metal Working and Material Science*, 2026, vol. 28, no. 2, pp. 280–297. DOI: 10.17212/1994-6309-2026-28.2-280-297. (In Russian).

Introduction

Tungsten carbide-cobalt cemented carbides are widely used as tool materials due to their exceptionally high hardness, wear resistance, and fracture toughness compared to other hard materials [1–4]. In particular, cemented carbides are used in the production of dies for industrial-scale manufacturing. Reducing the manufacturing cost of cemented carbide die components and improving the characteristics of the powders

*** Corresponding author**
Mikhailenko Elena A., Ph.D. (Physics and Mathematics), Senior researcher
Khabarovsk Federal Research Center FEB RAS,
153 Tihookeanskaya Str.,
680042, Khabarovsk, Russian Federation
Tel.: +7 4212 22-69-56, **e-mail:** mea80@list.ru

used are relevant issues [5]. The cost and properties of *WC*-based cemented carbides depend significantly on the properties of the binder metal.

Cobalt is often used as a binder for *WC*-based cemented carbide, but it has several disadvantages. These include primarily its high market cost due to increased demand for cobalt for battery production [6] and the toxicity of both cobalt itself (hazard class 2 according to GOST 9721-79) and its mixture with tungsten carbide powder [7, 8].

Fe and *Ni*, as well as *Co*, belong to group VIII of the periodic table and can be ideal alternative binder materials [9]. Moreover, a binder phase made of a medium-entropy Fe-Ni-Co alloy increases the fracture toughness of the cemented carbide [10]. Replacing part of the cobalt with nickel and iron is aimed primarily at improving the binder properties and reducing the cost of cobalt powder in cemented carbide production. However, most studies focus on the production and investigation of the microstructure [11, 12] and fundamental mechanical properties (hardness, strength, fracture toughness) of alloys with modified binder compositions [13–19]. To solve the problem of replacing the binder component in the production of cemented carbide dies, it is necessary to conduct a comparative analysis of the phase composition, microstructure, density, hardness, fracture toughness, strength, and wear resistance of the tungsten-cobalt alloy (*WC-Co*) and its analogue with a medium-entropy binder (*WC-Fe-Ni-Co*).

An additional factor increasing the cost of carbide tooling is the need for complex and expensive electrical discharge machining. Electrical discharge machining requires expensive machines (costing from 600,000 rubles) and a *CuW* electrode, and the material loss during processing of the carbide workpiece is significant. Modern studies demonstrate the possibility of obtaining products of complex configuration using 3D printing methods. Their manufacture requires 3D printers costing from 50,000 rubles, and the loss of starting material is less, as there is no need to make allowances for electrical discharge machining.

Products obtained by selective laser sintering or melting [12, 19–25] often have inferior properties compared to those obtained by conventional technology due to residual porosity and undesirable phase transformations caused by the need for heating above 2,000 °C, leading to tungsten carbide decomposition. The use of binder jetting [26–28] and extrusion technologies [29] for 3D printing of blanks from powder-polymer mixtures is hindered by the low flowability of the compositions and, consequently, insufficient density of the semi-finished products.

A promising method is the use of polymer dies manufactured by 3D printing methods for forming cemented carbide blanks followed by their sintering [30–34]. This method combines low cost (due to the use of inexpensive 3D printing methods) with high product characteristics (due to the high density of the blanks). The main problems with the application of this method remain the low rigidity and limited accuracy of plastic die components obtained by photopolymer 3D printing, which compromises the accuracy of cemented carbide blanks and products. It is necessary to verify the possibility of applying this method to obtain cemented carbide die components used in powder metallurgy. In particular, it is necessary to verify that an *SNUM-120408* cutting insert manufactured using a die obtained by this method meets the requirements of existing standards.

The aim of this work is to investigate the possibility of using additive technologies for forming die blanks from *WC-15Co* and *WC-5Fe-5Ni-5Co* alloys and to conduct a comparative analysis of the phase composition, microstructure, density, hardness, fracture toughness, strength, and wear resistance of these materials.

To achieve this aim, the following ***tasks*** were addressed during the research:

– to determine the phase composition, microstructure, density, hardness, fracture toughness, strength, and microabrasive wear resistance of *WC-15Co* and *WC-5Fe-5Ni-5Co* alloys and to conduct a comparative analysis;

– to verify the compliance of the main dimensions of *SNUM-120408* cutting inserts made of *WC-6Co* cemented carbide, manufactured using experimental cemented carbide dies, with the requirements of *GOST 19052-80* and *GOST 19042-80*, and to compare them with the dimensions of a commercial cutting insert.

For the first time, this work uses photopolymer dies to manufacture punch and die blanks for dies made of cemented carbide with an alternative binder in the form of a *Co–Fe-Ni* solid solution. This approach significantly simplifies the procedure for manufacturing dies for powder metallurgy.

Methods

For the creation of all samples, a medium-grain *WC* powder (grade *WC3*, *KZTS*, Russia) was used. A photograph of the *WC* powder and its particle size distribution is shown in Fig. 1. Cobalt (grade *PK-1E*, *GOST 9721-79*, Russia), nickel (*PNK-UT3*, *GOST 9722-97*), and iron (*ZhKV*, *TU 6-05-0210316-007-88*) powders were used as a binder.

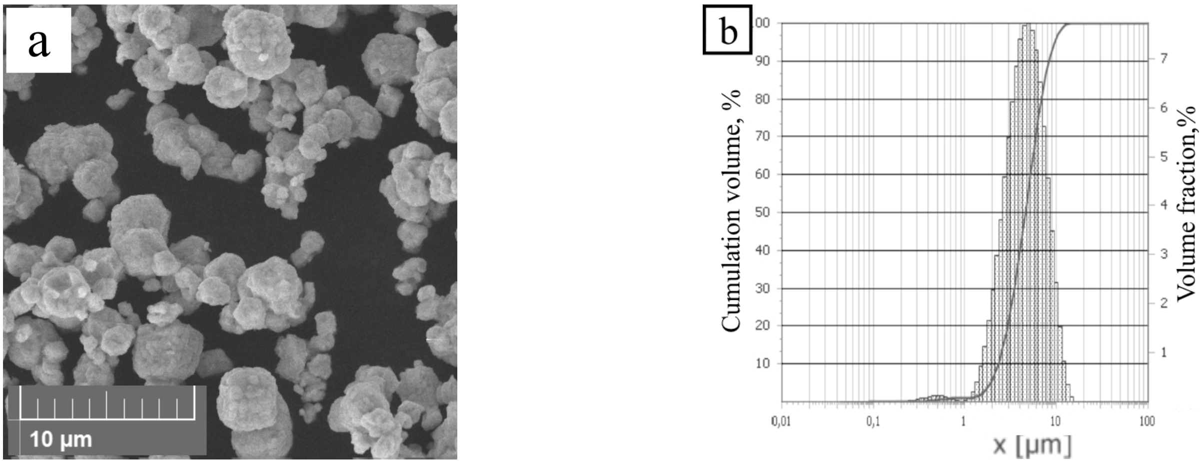

Fig. 1. Photograph of powder particles and particle size distribution of *WC* powder

Preparation of two batches (240 g each) of *WC-15Co* and *WC-5Fe-5Ni-5Co* compositions was carried out in a *Retsch PM-400* ball mill. The process lasted 1 hour at a rotation speed of 250 rpm in tungsten carbide jars with balls (ball-to-powder ratio 5:1). To improve formability, 1.5 wt.% rubber (as a 5 wt.% solution in petrol) was added to the mixture. After drying, the mixture was granulated by rubbing through a sieve.

From a portion of the obtained granules, bar-shaped samples (24 × 8 × 8 mm, weight 10 g) for standard tests were compacted in a steel die at a pressure of 200 MPa. The remaining material was used for pressing tooling components in photopolymer dies at a pressure of 50 MPa to avoid damaging the latter, since it was previously determined that increasing the pressing pressure in photopolymer dies from 50 to 200 MPa has little effect on the properties of the finished cemented carbide products [32].

The powder mixture for obtaining *SNUM-120408* cutting inserts (*WC-6Co* cemented carbide) was prepared similarly from *WC* and *Co* powders (total weight 30 g, mixing time 1 h).

A 3D model of the *SNUM-120408* cutting insert was developed in accordance with the requirements of *GOST 19052-80* (Fig. 2, *a*). Next, a 3D model of the cutting insert blank was developed based on the previously determined shrinkage of *WC-6Co* alloy blanks during sintering. 3D models of the die and punch blanks for the cemented carbide die (Figs. 2, *b, c*) were developed considering the shrinkage of the die component blanks during sintering and an allowance of 0.1 mm for diamond grinding. The shrinkage of the die components was calculated based on the ratio of the material density of the blanks after plasticizer removal to the theoretical density of the *WC-15Co* and *WC-5Fe-5Ni-5Co* alloys.

The die components were manufactured using photopolymer 3D printing on a *PhrozenSonicMini 8K* 3D printer. The layer height during 3D printing was 20 µm.

The process diagrams for forming using plastic tooling (made of *Water-Wash Resin 2.0*, *Anycubic*, China) are shown in Figs. 2, *d, e*. Fig. 2, *f* shows the finished main parts of the photopolymer die.

Punch blanks weighing 15 g (Fig. 2, *b*) and die blanks weighing 210 g each (Fig. 2, *c*) were pressed from granules obtained from *WC-15Co* and *WC-5Fe-5Ni-5Co*. Bar blanks were pressed in a steel die at

Fig. 2. Three-dimensional models of:
a – cutting insert blank; *b* – cemented carbide punch; *c* – carbide die; *d* – Diagram of pressing die blanks; *e* – diagram of pressing punch blanks; *f* – Components of the photopolymer die for producing cemented carbide die blanks; *g* – *WC-15Co* alloy die blank after pressing

a pressure of 200 MPa. The die component blanks were pressed from *WC-15Co* (Fig. 2, *g*) and *WC-5Fe-5Ni-5Co* alloys in plastic dies at a pressure of 50 MPa to avoid damaging the photopolymer die parts and significant deformation of the blanks.

Cutting insert blanks weighing 8.5 g each were pressed in dies made of *WC-15Co* and *WC-5Fe-5Ni-5Co* alloys at a pressure of 200 MPa. Four cutting inserts were manufactured, two in each die.

Then, all die blanks were placed in a *Carbolite STF* furnace, and the plasticizer was removed in an argon atmosphere during heating from 20 °C to 700 °C at a rate of 1–4 °C/min. Final sintering was performed under vacuum at a maximum temperature of 1,400 °C for one hour in the same furnace after cleaning. Sintering of the *WC-6Co* cemented carbide cutting inserts was carried out in the same furnace for one hour at a temperature of 1,450 °C.

After sintering, the bars were ground and polished to meet the dimensions 20 × 6.5 × 5.25 mm according to *ISO 3327:2009* and for further study of microstructure, hardness, and strength. The surfaces of the die components were ground and polished to reduce roughness. Microstructure and hardness were studied on the prepared samples.

The density of the obtained samples was determined by hydrostatic weighing using analytical scales (*Vibra Shinko Denshi*) with a density determination kit. Each sample was measured three times after drying. Strength assessment during testing of one bar for each composition was performed on an *IP-250M* testing machine according to *GOST 20019-74*. The phase composition was studied using a *DRON-7M* X-ray diffractometer. Hardness was determined using an *HVS-50* hardness tester at a load of 30 kgf based on five measurements for each sample.

The *WC* grain size was determined by the linear intercept method (*ASTM E112-24*) on microstructural photographs based on the analysis of more than 300 grains.

Wear resistance tests were carried out according to the “free ball-plane” scheme using a *Calotest* instrument (*CSM Instruments*, Switzerland) in accordance with the scheme presented in [35]. The samples were placed at an angle of 40 ° relative to the vertical plane. A carbide ball weighing 59.72 g and 20 mm in diameter was used as a counterbody. A suspension of fine aluminum oxide abrasive particles (average particle size 5 µm) in mineral oil at a mass ratio of 1:10 was used as the abrasive medium. The flow rate of the suspension into the contact zone between the ball and the sample was 0.005 mL/min (one drop every

10 minutes). The duration of each microabrasive wear test was 30 minutes. Each measurement was performed three times. The linear speed of the counterbody at the contact point was 0.51 m/s. The distance traveled in 30 minutes was $\boldsymbol{L}$ = 918 m.

The wear volume during tests was determined as the volume of the crater ($\boldsymbol{V}$) in the shape of a spherical segment with base diameter $\boldsymbol{d_c}$ and height $\boldsymbol{h}$:

$$V = \pi h^2 \left(\frac{d_c^2}{8h} + \frac{h}{6} \right), \quad (1)$$

The crater diameter $\boldsymbol{d_c}$ and height $\boldsymbol{h}$ were measured on the profile of the central section of the crater obtained using a profilometer. The specific wear of all materials was calculated using formula (2):

$$\mathbf{w} = \frac{V}{PL}, \quad (2)$$

where $\boldsymbol{P}$ = 0.415 N is the normal load.

After the wear resistance testing, the profiles of the formed craters were studied using a *Time Group Inc TR200* profilometer. The microstructure of the sample surfaces and the formed craters was studied using an *Altami MET 3 APO* optical microscope and a *Tescan Vega* scanning electron microscope. The compositions of the ground surfaces and craters were studied by *EDS* using an *Oxford X-Max* 80 detector.

Measurements of the dimensions of the manufactured cutting inserts were carried out using an optical microscope and an *MK-25* micrometer (error 4 μm). Measurements on different samples and different faces of the inserts were performed three times for each dimension. Confidence intervals for all measurements were calculated with a confidence level of 0.95 using *Student's t*-distribution.

A cutting insert *SNUM-120408* (*GOST 19052-80*) made of *WC-8Co* cemented carbide was used as a reference sample for dimensional comparison.

Results and discussion

Density and shrinkage of bars and die components

Based on the results of measuring the density of the bar blanks, the shrinkage of the samples was calculated: 21.6% for *WC-15Co* and 21.7% for *WC-5Fe-5Ni-5Co*.

As a result of sintering, bar samples of *WC-15Co* and *WC-5Fe-5Ni-5Co* alloys were obtained, with densities of 13.99 ± 0.01 g/cm^3 and 13.88 ± 0.01 g/cm^3, respectively. The theoretical density, usually calculated using the rule of mixtures (*ASTM B311-17*) for these alloys ($\boldsymbol{\rho}_{WC}$ = 15.65 g/cm^3, $\boldsymbol{\rho}_{Fe}$ = 8.87 g/cm^3, $\boldsymbol{\rho}_{Co}$ = 8.90 g/cm^3, $\boldsymbol{\rho}_{Ni}$ = 8.90 g/cm^3), is estimated (without considering the solubility of carbon and tungsten in the metallic binder) to be approximately 14.05 g/cm^3.

In this case, the relative density of the obtained alloys is 99.6% for *WC-15Co* and 98.8% for *WC-5Fe-5Ni-5Co*, which corresponds to the density of the *WC-Fe-Ni-Co* alloy (99%) reported in [36]. The density of the *WC-15Co* alloy was higher because cobalt wets tungsten carbide better than iron and nickel. The adhesion energies of *Fe*, *Ni*, *Ni-Co*, *Ni-Fe*, *Fe-Ni-Co* layers and *WC*, calculated by computer modeling methods based on density functional theory [37–40] and presented in Table 1, are lower than the adhesion energy of cobalt layers and tungsten carbide.

Based on the different relative densities, the porosity of the *WC-15Co* alloy bars was lower (0.4%) than that of the *WC-5Fe-5Ni-5Co* alloy samples (1.2%). Determining porosity by relative density allows one to approximately estimate the porosity of the samples. *GOST 3882-74* permits density deviations of up to 2.5%. At the same time, an increase in porosity negatively affects the hardness and strength of cemented carbides.

The shape and dimensions of the obtained experimental die components satisfy the requirements for a carbide die (Fig. 3). The density of the *WC-15Co* die was 13.92 ± 0.02 g/cm^3, and that of the *WC-5Fe-5Ni-5Co* die was 13.81 ± 0.02 g/cm^3.

Table 1

Adhesion energies of metallic bonds to the *WC* surface calculated using computer modeling methods

Metallic bond in the cement carbide	Adhesion energy (J/m^2)	Reference
Fe	3.44	[37]
Ni	4.61	[38]
Co	6.85–8.78	[39] [40]
Ni-Fe	4.688–4.809	[38]
Ni-Co	4.72–4.786	[38]
Fe-Ni-Co	6.574	[40]

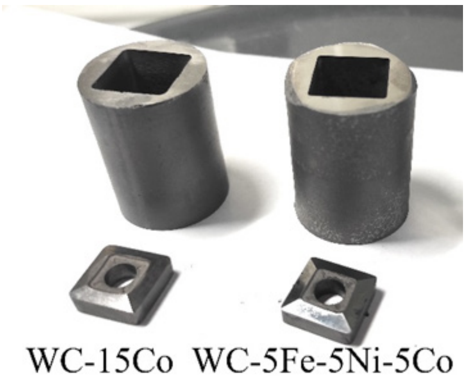

Fig. 3. Photograph of the obtained die components made of *WC-15Co* and *WC-5Fe-5Ni-5Co* cemented carbides

It was previously established that the pressing pressure has an insignificant effect on the density of cemented carbide products obtained using plastic dies [32, 33]. Therefore, despite the lower pressing pressure, the relative density of the die components made of *WC-15Co* (99.1%) and *WC-5Fe-5Ni-5Co* (98.3%) alloys was slightly lower than the density of the bars. The deviations in relative density of the die components (0.9% and 1.7%) are within the tolerance of *GOST 3882-74*.

The slight decrease in density is attributed to the greater height of the products and greater unevenness in density distribution within the die component blanks, which results from increased friction between the blank and the walls of the plastic die during pressing.

Phase composition, microstructure, and mechanical properties of WC-15Co and WC-5Fe-5Ni-5Co cemented carbides

The phase composition of the obtained alloys differs only in the position of the cobalt phase peak in the *WC-15Co* alloy and the *Fe-Ni-Co* solid solution peak in the *WC-5Fe-5Ni-5Co* alloy (Fig. 4). While in the *WC-15Co* alloy the peak position strictly corresponds to the *FCC* phase of cobalt, in the *WC-5Fe-5Ni-5Co* alloy a significant decrease in intensity and a slight shift are observed. This occurs due to the formation of a multi-component disordered solid solution consisting of iron, nickel, and cobalt atoms. A slight change in the relative intensities of the *WC* crystal lattice peaks is observed, which can be explained by the different shapes of the crystals formed during sintering as a result of recrystallization through the liquid phase.

Microstructural analysis confirmed (Fig. 5) that the obtained alloys consist only of binder and *WC* grains. No individual phases were detected in the *WC-5Fe-5Ni-5Co* alloy. This confirms the formation of a homogeneous solid solution consisting of iron, nickel, and cobalt atoms. Nevertheless, the *WC* grains in the *WC-5Fe-5Ni-5Co* alloy deviate significantly more from the regular shape than those in the *WC-15Co* alloy. This is because the grain growth rate by recrystallization through the liquid phase in the *WC-5Fe-5Ni-5Co* alloy is lower, and accordingly, grain growth and the formation of regular facets in such an alloy are slower.

Compared to the cobalt binder, the multi-component binder suppresses *WC* grain growth due to the retarded diffusion effect. It is known that the average *WC* grain size decreases with an increase in the content of the multi-component binder [41]. This explains the redistribution of the heights of the *WC* phase peaks in Fig. 4.

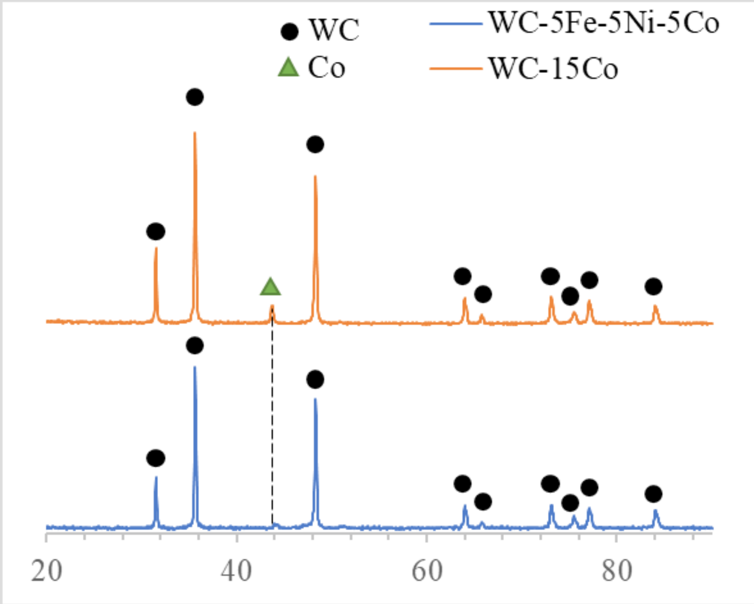

Fig. 4. Phase composition of the obtained alloys

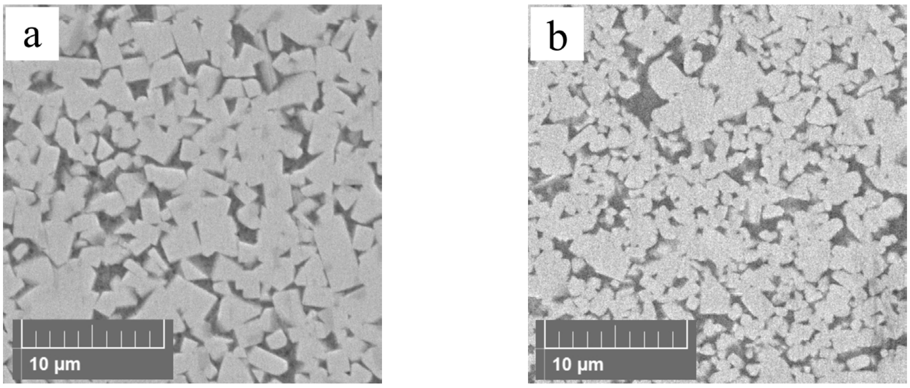

Fig. 5. Microstructures of (*a*) *WC-15Co* and (*b*) *WC-5Fe-5Ni-5Co* cemented carbides

According to literature data, the hardness of *Co* and *Fe-Ni-Co* (160–260 HV) is approximately the same [42]. Due to the smaller grain size (1.18 µm), the hardness of the *WC-5Fe-5Ni-5Co* alloy (1,070 ± 20 HV) was higher than that of the *WC-15Co* alloy (1,010 ± 30 HV), whose average *WC* grain diameter was 1.40 µm. This roughly corresponds to the difference in hardness of alloys with *Co* and *Fe-Ni-Co* binders observed in other studies [43].

Preliminary tests of two samples yielded close strength values (2,180 MPa for *WC-15Co* and 1,970 MPa for *WC-5Fe-5Ni-5Co*), which supports the hypothesis that there are no sharp differences in strength. However, additional studies are required for a statistically significant conclusion.

Wear tests showed that the average diameter and depth of craters in samples made of *WC-5Fe-5Ni-5Co* alloy (Figs. 6, *d*–6, *e*, 7, *b*) are smaller than those in samples made of *WC-15Co* alloy (Figs. 6, *a*–6,*b*, 7,*a*). This is primarily due to the smaller grain size and higher hardness of the *WC-5Fe-5Ni-5Co* alloy.

In the microstructure of the crater of the *WC-15Co* alloy (Fig. 6, *c*), it can be seen that cobalt is almost completely removed as a result of the abrasive action of the aluminum oxide particles. In the microstructure of the crater surface of the *WC-15Co* hard alloy, many large *WC* grains are visible, partially affected by the abrasive. That is, a significant part of the grains are torn out as a result of intergranular fracture under the action of the abrasive.

At the same time, in the microstructure of the crater of the *WC-5Fe-5Ni-5Co* alloy (Fig. 6, *f*), there are significantly more *WC* grains with traces of abrasive action, which indicates a predominantly transgranular

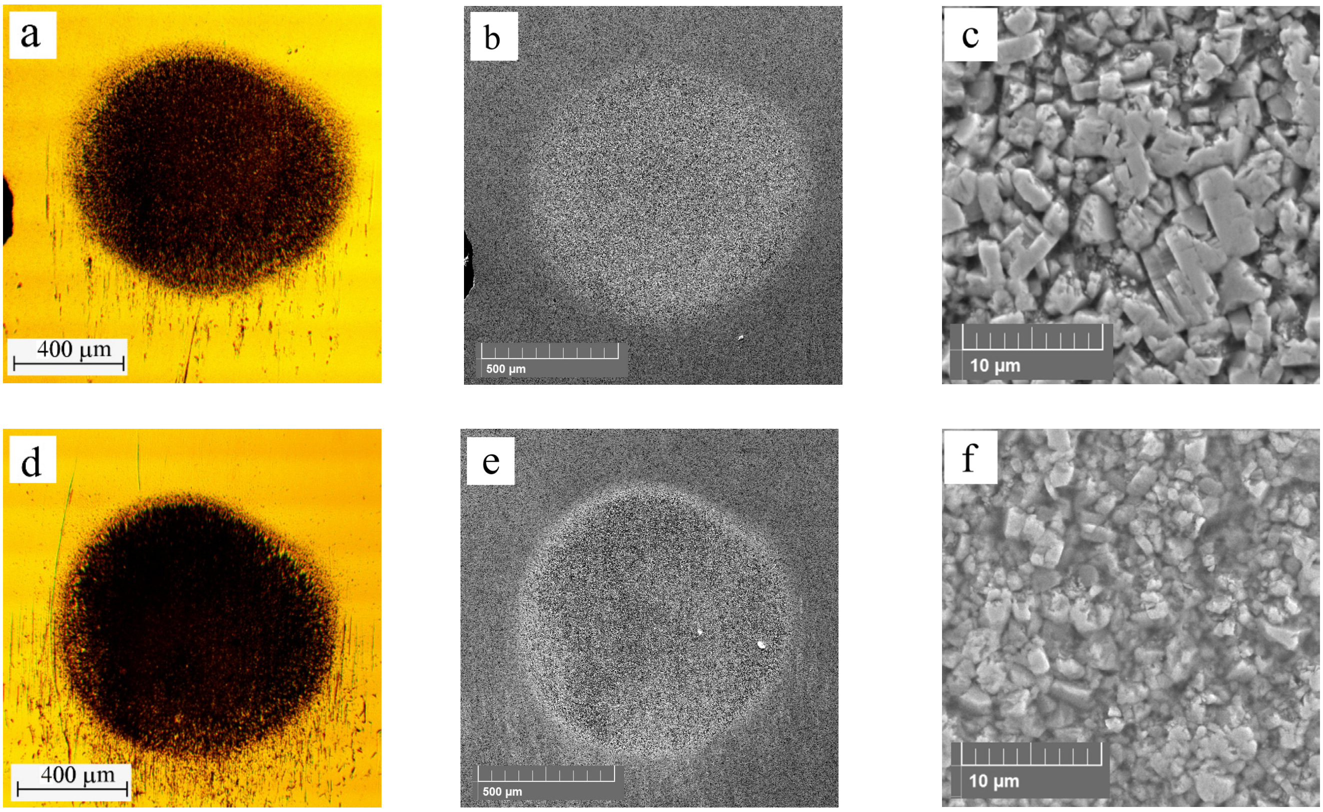

Fig. 6. Photographs of wear craters after microabrasive wear in the *WC-15Co* (*a–c*) and *WC-5Fe-5Ni-5Co* (*d–f*) cemented carbide specimens, obtained using optical (*a*, *d*) and scanning electron microscopes (*b*, *c*, *e*, *f*)

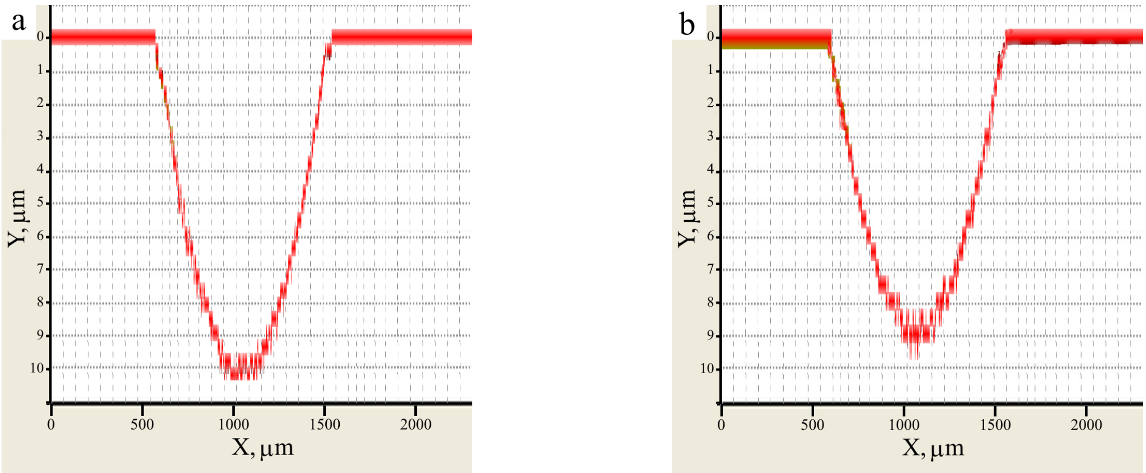

Fig. 7. Wear crater profiles of (*a*) *WC-15Co* and (*b*) *WC-5Fe-5Ni-5Co* cemented carbide specimens

fracture mechanism. Moreover, in this sample (Fig. 6, *f*), the size of the indentations between WC grains formed as a result of binder removal is noticeably smaller than in the *WC-15Co* alloy (Fig. 6,*c*).

The concentrations of metals in the *WC-15Co* alloy (Fig. 8, *a*) and in the *WC-5Fe-5Ni-5Co* alloy (Fig. 8,*c*), taking into account the presence of carbon in the required concentration, are close to the declared compositions. The carbon concentration was not determined, since energy-dispersive X-ray spectroscopy (*EDS*) gives too low accuracy for this component.

In the crater surfaces formed as a result of microabrasive wear, the concentration of binder metals (*Co*, *Fe*, *Ni*) decreases in both alloys, which corresponds to the observed microstructural changes (Figs. 6, *c*, *f*). At the same time, the relative concentration of cobalt (excluding carbon) in the *WC-15Co* alloy decreases

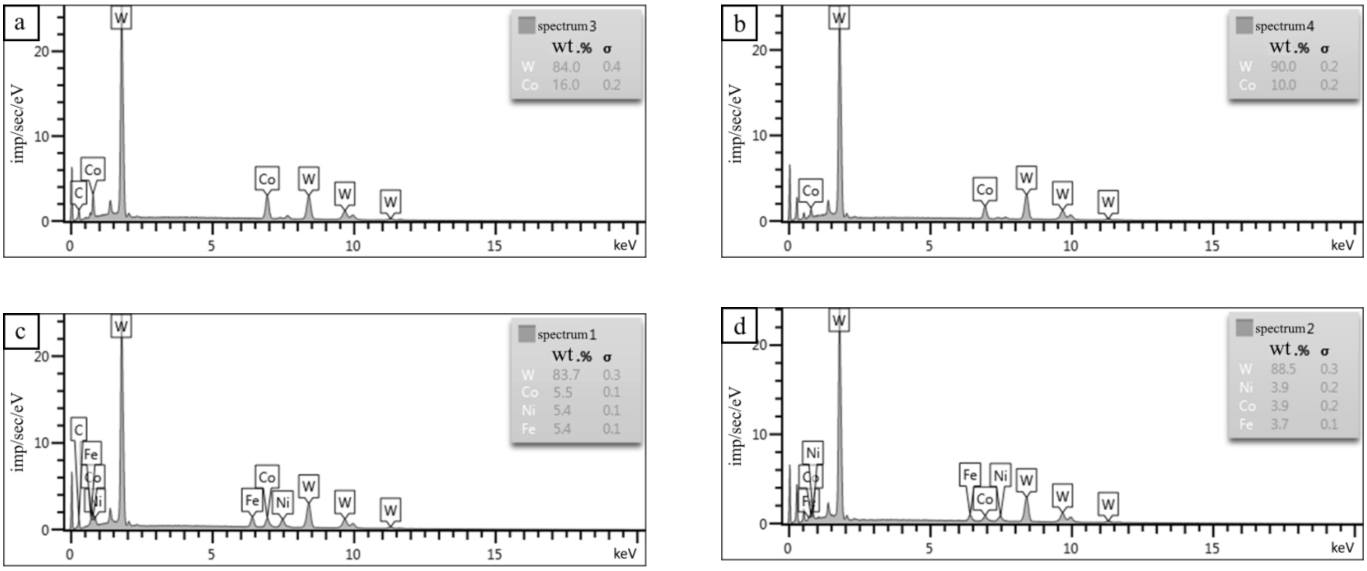

Fig. 8. Spectra of the initial (*a*, *c*) and worn (*b*, *d*) surfaces of *WC-15Co* (*a*, *b*) and *WC-5Fe-5Ni-5Co* (*c*, *d*) cemented carbide samples

from 16.0 to 10.0%. The total relative concentration of binder metals (*Fe*, *Ni*, *Co*) in the *WC-5Fe-5Ni-5Co* alloy decreases from 16.5 to 11.5%. Thus, the relative decrease in binder concentration in the *WC-5Fe-5Ni-5Co* alloy (30.3%) is 7.2% lower than that in the *WC-15Co* alloy (37.5%). This confirms that in the *WC-5Fe-5Ni-5Co* alloy, the binder is removed to a shallower depth due to its higher hardness.

Increased hardness and decreased *WC* grain size contribute to the increase in wear resistance of cemented carbides under microabrasive wear [1, 2]. Due to its higher hardness and smaller grain size, the wear rate of the alloy with the multi-component binder (*WC-5Fe-5Ni-5Co*) was 10% lower than that of the *WC-15Co* alloy (Fig. 9). However, this change in wear rate does not exceed the measurement error.

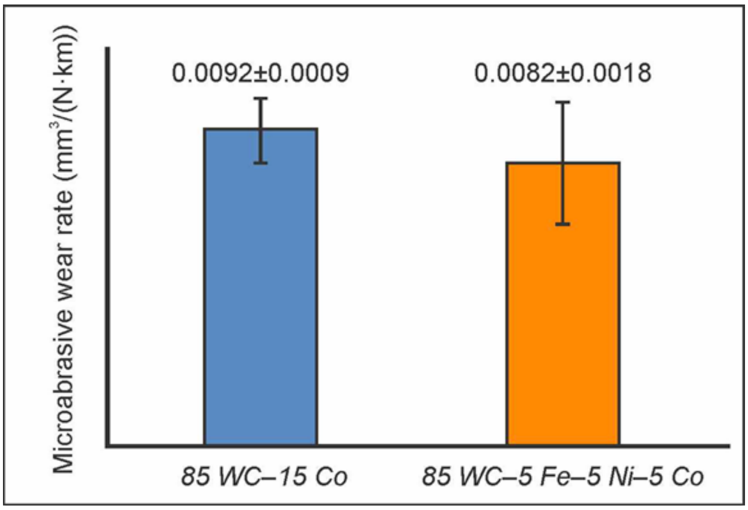

Fig. 9. Comparison of the microabrasive wear rate of cemented carbide specimens

Testing of the obtained dies

Both experimental cemented carbide dies for manufacturing blanks of *WC-6Co* cemented carbide *SNUM-120408* inserts were successful (Fig. 10). The obtained inserts comply with the density (14.85 ± ± 0.01 g/cm^3) and hardness (1,380 ± 10 HV) requirements of *GOST 3882-74*.

It is practically impossible to externally distinguish the inserts manufactured using the die made of *WC-5Fe-5Ni-5Co* alloy from those manufactured using the die made of *WC-15Co* alloy (Fig. 10). It can be

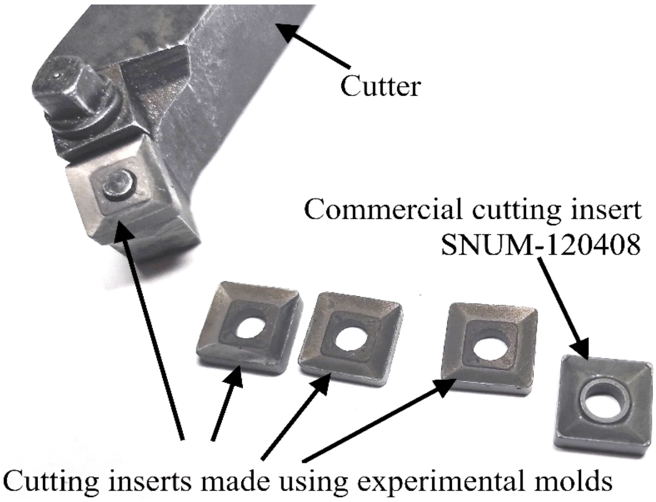

Fig. 10. Cutting inserts manufactured using experimental dies and a commercial counterpart

expected that, due to its higher wear resistance, the service life of the die made of *WC-5Fe-5Ni-5Co* alloy under low-intensity abrasive wear conditions will be higher than that of the die made of *WC-15Co* alloy.

The dimensions of the obtained inserts comply with *GOST 19052-80*. Fig. 11 shows an example of the required corner radius (0.8 mm) of *SNUM-120408* cutting inserts.

Fig. 11, *a* shows that the high precision of 3D printing ensured the required corner radius of the photopolymer die, calculated by considering the shrinkage of the die and the product blank (21.6% for *WC-Co* and 21.7% for *WC-5Fe-5Ni-5Co*, respectively) during sintering (1.19 = 0.8 × 1.22 × 1.22).

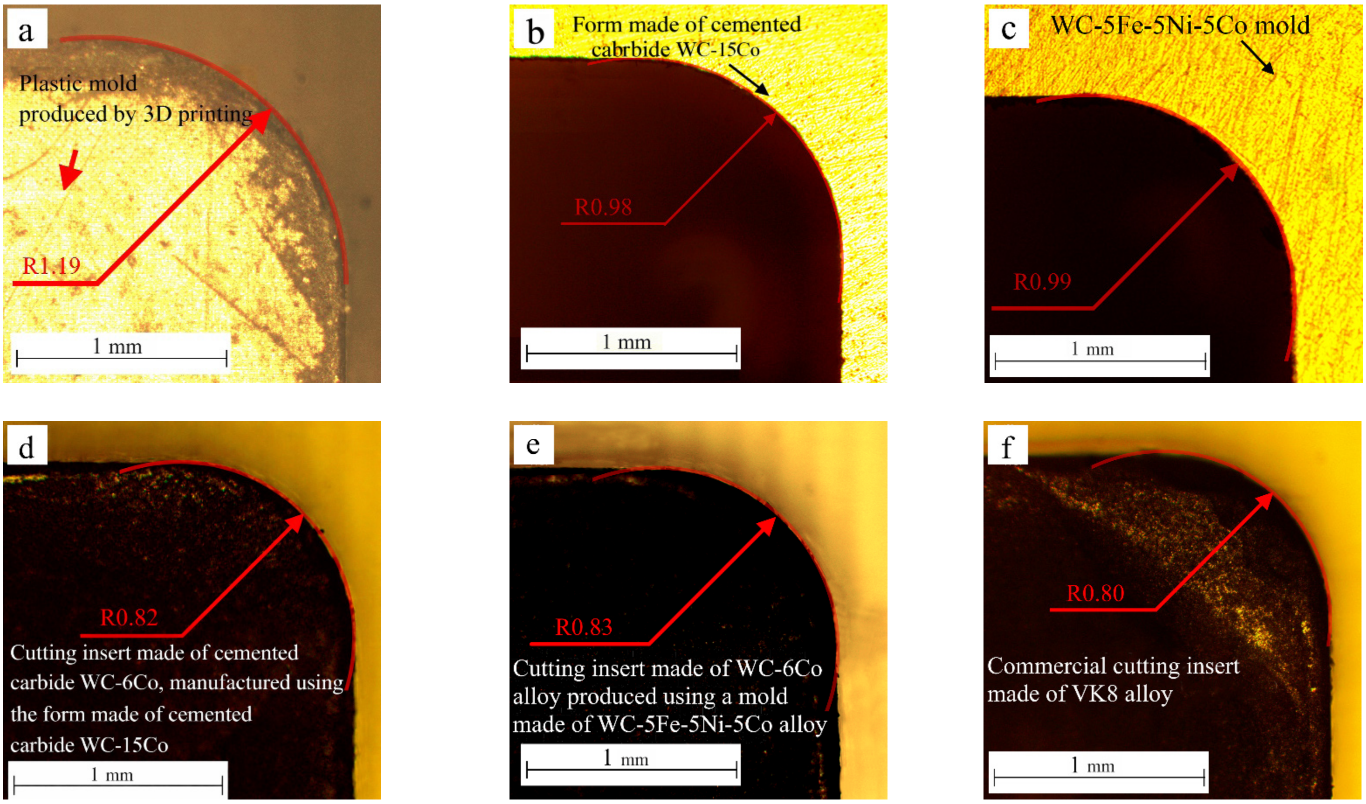

Fig. 11. (*a*) Photograph of the rounded plastic die for pressing a die blank obtained by 3D printing; (*b*) Photograph of die for pressing cutting insert blanks from the *WC-15Co* cemented carbide; (*c*) Photograph of die for pressing cutting insert blanks from the *WC-5Fe-5Ni-5Co* cemented carbide; (*d*, *e*) Corner rounding of the manufactured cutting inserts; (*f*) Corner rounding of a commercial cutting insert

Fig. 11, *b* shows that the sintered die made of *WC-15Co* alloy has a corner radius close to the planned value, considering further shrinkage of the cutting insert blank (0.98 = 0.8 × 1.22).

The corner radius of the die made of *WC-5Fe-5Ni-5Co* alloy (Fig. 11, *c*) was slightly larger (0.99 mm) due to the lower shrinkage of the die.

The corner radii of the cutting inserts obtained after pressing the blanks in dies made of *WC-15Co* (Fig. 11, *d*) and *WC-5Fe-5Ni-5Co* (Fig. 11,*e*) alloys were slightly larger than planned (0.82 and 0.83 mm instead of 0.80 mm) due to the difficulty of predicting shrinkage during sintering of experimental samples.

Nevertheless, the obtained cutting inserts are close in corner radius and other main dimensions to the required dimensions (*GOST 19052-80*, considering the tolerances of *GOST 19042-80*) and differ little in their main dimensions (Table 2) from a similar commercial insert (Fig. 11, *f*). Tolerances for the hole diameter and corner radius were not found.

Table 2

Dimensional characteristics of *SNUM-120408* cutting inserts

Die material	Cutting edge length, ***l*** (mm)	Thickness, ***s*** (mm)	Hole diameter, d_1 (mm)	Corner radius, ***r*** (mm)
WC-15Co	12.82±0.01	4.78±0.01	5.15±0.05	0.82
WC-5Fe-5Ni-5Co	12.80±0.01	4.78±0.01	5.15±0.05	0.83
Commercial *WC – 8 Co* insert	12.62±0.01	4.84±0.01	4.85±0.05	0.8
GOST 19052-80, GOST 19042-80	12.7±0.13	4.76±0.13	5.16	0.8

Conclusion

This work experimentally confirmed the effectiveness of a combined approach to manufacturing carbide tooling that integrates inexpensive photopolymer 3D printing of dies with subsequent cold pressing and vacuum sintering.

1. Despite the lower pressing pressure (50 MPa) in photopolymer dies compared to steel dies (200 MPa), the relative density of the obtained die components (weighing up to 210 g) made of *WC-15Co* and *WC-5Fe-5Ni-5Co* alloys was 99.1% and 98.3%, respectively. These values are slightly lower than the density of reference samples but meet the requirements of *GOST 3882-74*.

It was found that replacing the traditional cobalt binder with a medium-entropy *Fe-Ni-Co* binder in the *WC-5Fe-5Ni-5Co* alloy leads to changes in the mechanical properties. The lower adhesion energy and retarded diffusion in the multi-component binder suppress *WC* grain growth (1.18 µm vs. 1.40 µm for *WC-15Co*). This, together with the higher hardness of the binder itself, increases the hardness of the alloy (1,070 HV vs. 1,010 HV). This, in turn, causes a decrease in the microabrasive wear rate by 10% (within the measurement error) compared to the *WC-15Co* alloy. At the same time, the *WC-15Co* alloy demonstrates higher density (99.6%) and flexural strength (2,180 MPa vs. 1,970 MPa).

It is shown that the microabrasive wear mechanism of the studied alloys differs. In the *WC-15Co* alloy, intergranular fracture with grain pull-out and intensive binder removal (cobalt concentration decrease by 37.5%) predominates. In the *WC-5Fe-5Ni-5Co* alloy, wear is predominantly transgranular with a shallower depth of binder removal (decrease in total *Fe-Ni-Co* concentration by 30.3%), which confirms its increased resistance to abrasive action.

2. The practical significance of this work is confirmed by the successful use of the dies made from both cemented carbides to produce *SNUM-120408* cutting inserts from *WC-6Co* cemented carbide. The geometric parameters of the inserts (cutting edge length 12.80–12.82 mm, thickness 4.78 mm, mounting hole diameter 5.15 mm, corner radius 0.82–0.83 mm), their density (14.85 g/cm^3), and hardness (HRA 89) are within the tolerances established by *GOST 19052-80*, *GOST 19042-80*, and *GOST 3882-74*, and correspond to the level of a similar commercial cutting insert. The die material did not have a significant impact on the quality of the finished products, while offering lower material cost due to the use of less valuable components.

References

1. Dvornik M.I., Mokritsky B.Ya., Zaitsev A.V. Sravnitel'nyi analiz mikroabrazivnoi iznosostoikosti traditsionnykh tverdykh splavov i submikronnogo tverdogo splava WC-8Co-1Cr_3C_2 [Comparative analysis microabrasive wear traditional submicron carbide and tungsten carbide WC-8Co-1Cr_3C_2]. *Voprosy materialovedeniya = Inorganic Materials: Applied Research*, 2015, no. 1 (81), pp. 45–51. (In Russian).

2. Dvornik M.I., Zaitsev A.V. Sravnitel'nyi analiz iznosostoikosti submikronnogo tverdogo splava WC-8Co-1Cr_3C_2 i traditsionnykh tverdykh splavov pri sukhom trenii [Comparative analysis of wear resistance of submicron hard alloy WC-8Co-1Cr_3C_2 and traditional hard alloys under dry friction]. *Perspektivnye materialy = Inorganic Materials: Applied Research*, 2015, no. 5, pp. 34–41. (In Russian).

3. *Efimovich I.A., Zolotukhin I.S., Zav'yalov E.S.* Temperaturnyi koeffitsient lineinogo rasshireniya vol'framokobal'tovykh tverdykh splavov [Thermal coefficient of linear expansion of tungsten-cobalt cemented carbide]. *Obrabotka metallov (tekhnologiya, oborudovanie, instrumenty) = Metal Working and Material Science*, 2019, vol. 21, no. 3, pp. 129–140. DOI: 10.17212/1994-6309-2019-21.3-129-140.

4. Toshov J.B., Fozilov D.M., Yelemessov K.K., Ruziev U.N., Abdullayev D.N., Baskanbayeva D.D., Bekirova L.R. Povyshenie stoikosti zub'ev burovykh dolot za schet izmeneniya tekhnologii ikh izgotovleniya [Increasing the durability of drill bit teeth by changing its manufacturing technology]. *Obrabotka metallov (tekhnologiya, oborudovanie, instrumenty) = Metal Working and Material Science*, 2024, vol. 26, no. 4, pp. 112–124. DOI: 10.17212/1994-6309-2024-26.4-112-124.

5. Belousova V.P., Popova M.N., Belousov A.L. Ekonomiko-tekhnologicheskie aspekty organizatsii proizvodstva izdelii iz poroshkovykh materialov na mashinostroitel'nykh predpriyatiyakh [Economic technological aspects of organization of articles production manufacture of wares under on nonspecialized machine-building enterprises]. *Konstruktsii iz kompozitsionnykh materialov = Composite Materials Constructions*, 2007, no. 4, pp. 122–126.

6. Gent W.E., Busse G.M., House K.Z. The predicted persistence of cobalt in lithium-ion batteries. *Nature Energy*, 2022, vol. 7 (12), pp. 1132–1143. DOI: 10.1038/s41560-022-01129-z.

7. Armstead A.L., Li B. Nanotoxicity: emerging concerns regarding nanomaterial safety and occupational hard metal (WC-Co) nanoparticle exposure. *International Journal of Nanomedicine*, 2016, vol. 11, pp. 6421–6433. DOI: 10.2147/IJN.S121444.

8. Armstead A., Li B. In vitro inflammatory effects of hard metal (WC-Co) nanoparticle exposure. *International Journal of Nanomedicine*, 2016, vol. 11, pp. 6195–6206. DOI: 10.2147/IJN.S121176.

9. Shichalin O.O., Buravlev I.Y., Papynov E.K., Golub A.V., Belov A.A., Buravleva A.A., Yudakov A.A. Comparative study of WC-based hard alloys fabrication via spark plasma sintering using Co, Fe, Ni, Cr, and Ti binders. *International Journal of Refractory Metals and Hard Materials*, 2022, vol. 102, p. 105725. DOI: 10.1016/j.ijrmhm.2021.105725.

10. Qian C., Li K., Chen S., Liu Y., Wang B., Liu Y. Fracture behavior of cemented carbides with CoNiFe medium entropy alloy binder. *International Journal of Refractory Metals and Hard Materials*, 2021, vol. 98, p. 105547. DOI: 10.1016/j.ijrmhm.2021.105547.

11. Gao Y., Luo B.H., He K.J., Jing H.B., Bai Z.H., Chen W., Zhang W.W. Mechanical properties and microstructure of WC-Fe-Ni-Co cemented carbides prepared by vacuum sintering. *Vacuum*, 2017, vol. 143, pp. 271–282. DOI: 10.1016/j.vacuum.2017.06.028.

12. Chang S.-H., Chang M.-H., Huang K.-T. Study on the sintered characteristics and properties of nanostructured WC-15 wt%(Fe-Ni-Co) and WC-15 wt% Co hard metal alloys. *Journal of Alloys and Compounds*, 2015, vol. 649, pp. 89–95. DOI: 10.1016/j.jallcom.2015.07.119.

13. Li H., Zhang H., Chen D., Jiang Z. Comparative study of the microstructure and mechanical properties of WC/High-speed steel composite materials prepared with Co, Ni, and Fe binders. *JOM*, 2024, vol. 76 (5), pp. 2120–2131. DOI: 10.1007/s11837-024-06429-1.

14. Soria-Biurrun T., Sánchez-Moreno J.M., Frisk K. Experimental and theoretical study of WC-40Fe-20Co-40Ni. *International Journal of Refractory Metals and Hard Materials*, 2022, vol. 102, p. 105719. DOI: 10.1016/j.ijrmhm.2021.105719.

15. Soria-Biurrun T., Sridar S., Frisk K., Xiong W., Sánchez-Moreno J.M. Experimental investigation and thermodynamic modelling of WC-Fe-Ni-Co-Cr cemented carbides. *International Journal of Refractory Metals and Hard Materials*, 2024, vol. 124, p. 106824. DOI: 10.1016/j.ijrmhm.2024.106824.

16. Wu J., Ren D., Xie B., He R., Geng Z., Zhang Z., Zhang W. Effect of Cr_3C_2 addition on microstructure and mechanical properties of WC-CoNiFe cemented carbides. *Metals*, 2024, vol. 14 (8), p. 895. DOI: 10.3390/met14080895.

17. Soria-Biurrun T., Lozada-Cabezas L., Navarrete-Cuadrado J., Ibarreta-Lopez F., Martinez-Pampliega R., Sanchez-Moreno J.M. Densification of WC-Fe-Ni-Co-Cr cemented carbides processed by HIP after sintering: effect of WC powder particle size. *International Journal of Refractory Metals and Hard Materials*, 2023, vol. 110, p. 105994. DOI: 10.1016/j.ijrmhm.2022.105994.

18. Ovcharenko A.G., Kozlyuk A.Yu., Kurepin M.O. Povyshenie iznosostoikosti plastin iz tverdogo splava [The increase of wear resistance for the hard-facing alloys plates]. *Obrabotka metallov (tekhnologiya, oborudovanie, instrumenty) = Metal Working and Material Science*, 2010, no. 2 (47), pp. 13–15.

19. Krinitcyn M., Svarovskaya N.V., Rodkevich N., Ryumin E., Lerner M. Structure and properties of WC-Fe-Ni-Co nanopowder composites for use in additive manufacturing technologies. *Metals*, 2024, vol. 14 (2), p. 167. DOI: 10.3390/met14020167.

20. Chen J., Huang M., Fang Z.Z., Koopman M., Liu W., Deng X., Zhao Z., Chen S., Wu S., Liu J., Qi W., Wang Z. Microstructure analysis of high density WC-Co composite prepared by one step selective laser melting. *International Journal of Refractory Metals and Hard Materials*, 2019, vol. 84, p. 104980. DOI: 10.1016/j.ijrmhm.2019.104980.

21. Li C.-W., Chang K.-C., Yeh A.-C. On the microstructure and properties of an advanced cemented carbide system processed by selective laser melting. *Journal of Alloys and Compounds*, 2019, vol. 782, pp. 440–450. DOI: 10.1016/j.jallcom.2018.12.187.

22. Gu D., Meiners W. Microstructure characteristics and formation mechanisms of in situ WC cemented carbide based hardmetals prepared by Selective Laser Melting. *Materials Science and Engineering: A*, 2010, vol. 527 (29–30), pp. 7585–7592. DOI: 10.1016/j.msea.2010.08.075.

23. Khmyrov R.S., Safronov V.A., Gusarov A.V. Synthesis of nanostructured WC-Co hardmetal by selective laser melting. *Procedia IUTAM*, 2017, vol. 23, pp. 114–119. DOI: 10.1016/j.piutam.2017.06.011.

24. Zhang L., Hu C., Yang Y., Misra R.D.K., Kondoh K., Lu Y. Laser powder bed fusion of cemented carbides by developing a new type of Co coated WC composite powder. *Additive Manufacturing*, 2022, vol. 55, p. 102820. DOI: 10.1016/j.addma.2022.102820.

25. Mostafaei A., De Vecchis P., Kimes K.A., Elhassid D., Chmielus M. Effect of binder saturation and drying time on microstructure and resulting properties of sinter-HIP binder-jet 3D-printed WC-Co composites. *Additive Manufacturing*, 2021, vol. 46, p. 102128. DOI: 10.1016/j.addma.2021.102128.

26. Mariani M., Goncharov I., Mariani D., De Gaudenzi G.P., Popovich A., Lecis N., Vedani M. Mechanical and microstructural characterization of WC-Co consolidated by binder jetting additive manufacturing. *International Journal of Refractory Metals and Hard Materials*, 2021, vol. 100, p. 105639. DOI: 10.1016/j.ijrmhm.2021.105639.

27. Kim H., Kim J.I., Kim Y.D., Jeong H., Ryu S.S. Material extrusion-based three-dimensional printing of WC–Co alloy with a paste prepared by powder coating. *Additive Manufacturing*, 2022, vol. 52, p. 102679. DOI: 10.1016/j.addma.2022.102679.

28. Mariani M., Mariani D., De Gaudenzi G.P., Lecis N. Effect of printing parameters on sintered WC-Co components by binder jetting. *European Journal of Materials*, 2022, vol. 2 (1), pp. 365–380. DOI: 10.1080/26889277.2022.2076617.

29. Rubiano Buitrago J.D., Gil Plazas A.F., Boyacá Mendivelso L.A., Herrera Quintero L.K. Fused filament fabrication of WC-10Co hardmetals: a study on binder formulations and printing variables. *Journal of Manufacturing and Materials Processing*, 2024, vol. 8 (3), p. 118. DOI: 10.3390/jmmp8030118.

30. Dvornik M.I., Mikhailenko E.A., Burkov A.A., Kolzun D.A. Dependence of density, hardness, strength, and dimensions of WC–15 Co hard alloy samples on the plasticizer content in workpieces obtained using a plastic mold made by 3D printing. *Inorganic Materials: Applied Research*, 2024, vol. 15 (5), pp. 1457–1465. DOI: 10.1134/S2075113324701132.

31. Dvornik M.I., Mikhailenko E.A., Burkov A.A., Chernyakov E.V. Vozmozhnost' ispol'zovaniya neraz"emnoi isparyaemoi plastikovoi formy, poluchennoi metodom 3D-pechati, dlya formovaniya tverdosplavnoi frezy [The possibility of using an evaporable plastic block mold made by 3D printing for forming a hard alloy milling cutter]. *Tsvetnye metally*, 2025, no. 8, pp. 36–41. DOI: 10.17580/tsm.2025.08.04. (In Russian).

32. Dvornik M.I., Mikhailenko E.A., Burkov A.A., Chernyakov E.V. Issledovanie kharakteristik rezhushchikh plastin iz tverdogo splava WC-5TiC-10Co, poluchennykh s primeneniem plastikovoi formy, izgotovlennoi metodom 3D-pechati [Investigation of the properties of wc-5tic-10co cutting inserts produced using a 3D-printed plastic mold]. *Izvestiya vysshikh uchebnykh zavedenii. Poroshkovaya metallurgiya i funktsional'nye pokrytiya = Powder Metallurgy and Functional Coatings*, 2024, vol. 18, no. 5, pp. 55–65. DOI: 10.17073/1997-308X-2024-5-55-65.

33. Dvornik M.I., Mikhailenko E.A., Burkov A.A., Kolzun D.A. 3D printed plastic molds utilization for WC-15Co cemented carbide cold pressing. *International Journal of Refractory Metals and Hard Materials*, 2023, vol. 115, p. 106312. DOI: 10.1016/j.ijrmhm.2023.106312.

34. Kim H., Kim J.I., Kim Y.D., Jeong H., Ryu S.S. Cast WC-Co alloy-based tool manufacturing using a polymeric mold prepared via digital light processing 3D printing. *Materials Letters*, 2022, vol. 306, p. 130979. DOI: 10.1016/j.matlet.2021.130979.

35. Dvornik M.I., Shichalin O.O., Mikhailenko E.A., Vlasova N.M., Chernyakov E.V. Dependence of wear rate of sintered WC and cemented carbides on hardness and cobalt content during free ball micro-abrasive wear test. *International Journal of Refractory Metals and Hard Materials*, 2025, vol. 134, p. 107495. DOI: 10.1016/j.ijrmhm.2025.107495.

36. Gao Y., Luo B.H., He K.J., Zhang W.W., Bai Z.H. Effect of Fe/Ni ratio on the microstructure and properties of WC-Fe-Ni-Co cemented carbides. *Ceramics International*, 2018, vol. 44 (2), pp. 2030–2041. DOI: 10.1016/j.ceramint.2017.10.149.

37. Shi Z., Liu S., Gao Y., Zhou Y., Wang Y., Liu Y. First-principles calculation on the relationships of h-WC/γ-Fe interface. *Journal of Physics and Chemistry of Solids*, 2018, vol. 123, pp. 11–18. DOI: 10.1016/j.jpcs.2018.07.006.

38. Lu K., Liu Y., Zhang H., Wang Z., Liu C., Zhou Y. Effect of solute elements (Cr, Mo, Fe, Co) on the adhesion properties of WC/Ni-based binder interface: A first-principles study. *International Journal of Refractory Metals and Hard Materials*, 2021, vol. 98, p. 105563. DOI: 10.1016/j.ijrmhm.2021.105563.

39. Gnidenko A.A. First principle simulation of the Co layers behavior on a surface of hexagonal tungsten carbide. *Physics Procedia*, 2012, vol. 23, pp. 132–135. DOI: 10.1016/j.phpro.2012.01.033.

40. Li H., Zhang H., Jiang Z. Investigation of the effect of partial Co substitution by Ni and Fe on the interface bond strength of WC cemented carbide based on first-principles calculations. *Materials Today Communications*, 2024, vol. 40, p. 109470. DOI: 10.1016/j.mtcomm.2024.109470.

41. Luo W., Liu Y., Luo Y., Wu M. Fabrication and characterization of WC-AlCoCrCuFeNi high-entropy alloy composites by spark plasma sintering. *Journal of Alloys and Compounds*, 2018, vol. 754, pp. 163–170. DOI: 10.1016/j.jallcom.2018.04.260.

42. Walbrühl M., Linder D., Agren J., Borgenstam A. A new hardness model for materials design in cemented carbides. *International Journal of Refractory Metals and Hard Materials*, 2018, vol. 75, pp. 94–100. DOI: 10.1016/j.ijrmhm.2018.04.004.

43. Qian C., Li K., Guo X.Y., Liu B., Long Z.Y., Liu Y. Effect of WC grain size on mechanical properties and microstructures of cemented carbide with medium entropy alloy Co-Ni-Fe binder. *Journal of Central South University*, 2020, vol. 27 (4), pp. 1146–1157. DOI: 10.1007/s11771-020-4355-5.

Conflicts of Interest

The authors declare no conflict of interest.